Reaction Chemistry & Engineering

Fast Microflow Kinetics and Acid Catalyst Deactivation in Glucose Conversion to 5-hydroxymethylfurfural

Journal:	*Reaction Chemistry & Engineering*
Manuscript ID	RE-ART-09-2020-000391.R1
Article Type:	Paper
Date Submitted by the Author:	24-Oct-2020
Complete List of Authors:	Chen, Tai-Ying; University of Delaware, Chemical and Biomolecular Engineering Cheng, Ziwei; University of Delaware, Chemical and Biomolecular Engineering Desir, Pierre; University of Delaware, Chemical and Biomolecular Engineering Saha, Basudeb; Catalysis Center for Energy Innovation; RiKarbon Inc, Vlachos, Dion; University of Delaware, Chemical and Biomolecular Engineering; Catalysis Center for Energy Innovation

Table of Contents Entry

Fast Microflow Kinetics and Acid Catalyst Deactivation in Glucose Conversion to 5-hydroxymethylfurfural

Tai-Ying Chen[a], Ziwei Cheng[a], Pierre Desir[a], Basudeb Saha[b,c], and Dionisios G. Vlachos[a,b,*]

[a]Department of Chemical and Biomolecular Engineering, University of Delaware, 150 Academy Street, Newark, Delaware 19716, United States

[b]Catalysis Center for Energy Innovation, 221 Academy Street, Newark, Delaware 19716, United States

[c]Current affiliation: RiKarbon Inc, 550 S. College Ave, Newark, Delaware 19716, United States

[*]Corresponding author; vlachos@udel.edu (D.G. Vlachos)

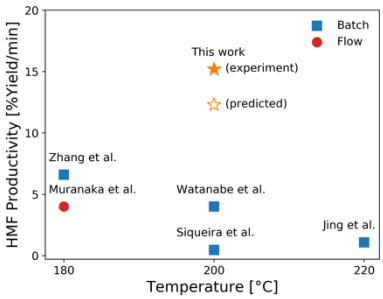

Continuous flow microreactors operating at short residence times and high temperatures can give high HMF productivity and contribute to process intensification of biorefineries.

Fast Microflow Kinetics and Acid Catalyst Deactivation in Glucose Conversion to 5-hydroxymethylfurfural

Tai-Ying Chen[a], Ziwei Cheng[a], Pierre Desir[a], Basudeb Saha[b,c], and Dionisios G. Vlachos[a,b,*]

[a]Department of Chemical and Biomolecular Engineering, University of Delaware, 150 Academy Street, Newark, Delaware 19716, United States

[b]Catalysis Center for Energy Innovation, 221 Academy Street, Newark, Delaware 19716, United States

[c]Current affiliation: RiKarbon Inc, 550 S. College Ave, Newark, Delaware 19716, United States

[*]Corresponding author; vlachos@udel.edu (D.G. Vlachos)

Abstract

5-hydroxymethyl furfural (HMF) is an important platform chemical because it can be upgraded to various drop-in and performance-advantaged products. The cascade reaction of HMF production from glucose over a Lewis acid ($CrCl_3$) and a Brønsted acid (HCl) catalyst in aqueous media is investigated in a microreactor at short residence times and high temperatures. We study the formation of various chromium species using UV-Visible spectrophotometry and elucidate the Cr(III) speciation. The catalyst reactivity increases sharply at short residence times, and then drops at long times. This indicates that the catalyst treatment plays a vital role in getting optimal reactivity, and recording the catalyst history is necessary. We develop a kinetic model to describe the catalyst speciation as well as the Lewis and Brønsted acid-catalyzed reaction kinetics using a hierarchical approach. The model is in good agreement with experiments. We demonstrate the benefits of tandem Lewis-external added Brønsted acid catalysis in processing time, productivity, and catalyst stability. We apply this model to optimize the HMF yield and obtain ~36% yield at 200 °C in 7 min and report the highest productivity of ~15% yield/min, demonstrating the opportunity of reaching high productivity at short residence times.

Keywords: acid catalysis, glucose conversion, 5-hydroxymethylfurfural, kinetic model, metal salts, UV-visible spectrophotometry

Introduction

Due to the growing environmental concerns, replacing fossil fuel-derived products with molecules derived from renewable lignocellulosic biomass has received increased attention.[1-6] As such, the conversion of biomass-derived carbohydrates, such as glucose and fructose, to platform molecules, including 5-hydroxymethyl furfural (HMF), has been studied extensively.[1-3, 7] A wide variety of catalysts,[8-10] solvents and solvent mixtures,[11-13] phase modifiers,[14] reaction conditions as well as reactor designs[15, 16] have been investigated to optimize the production of HMF. Recently, the application of microreactors to biomass processing, in particular the conversion of sugars to HMF, is receiving growing attention. This stems from their unique advantages, such as fast heat and mass transfer, precise temperature control, and the ability to study reaction kinetics under differential conversions where short residence times and precise process control render collection of large amounts of data feasible.[17-19] However, most microfluidic studies have used fructose as the substrate.[20-22] In comparison to fructose, glucose is an abundant and cheaper feedstock. However, achieving high HMF yield from glucose at short residence times with only Brønsted acid-catalyzed dehydration is challenging.[3, 23] Therefore, it is common to isomerize the glucose to fructose first and then dehydrate fructose into HMF.[1, 9, 24] The isomerization of glucose to fructose is an equilibrium-limited reaction with approximately unity equilibrium constant at room temperature.[25] Consequently, glucose conversion is modest.

To mitigate the limited conversion, combined Lewis/Brønsted acid catalysts are effective. The Lewis acid is active for isomerization of glucose to fructose[26, 27] and tolerates Brønsted acidity as well at high temperatures.[9] The fructose is simultaneously dehydrated to HMF in a single reactor. Various tandem Lewis/Brønsted acid catalysts, including both homogeneous and heterogeneous, have been applied to the production of HMF.[11, 28-34] While heterogeneous catalysts are easily separated from reaction solutions, the formation of undesired products, such as soluble polymers and humins can deposit in and block the catalyst pores, which requires frequent regeneration.[24] In this context, homogeneous catalysts for HMF production are meritorious. Moreover, homogeneous catalysts allow better mixing with the glucose reactant and are easier to use in the narrow micro-scale channels. Various metal salts catalyze the conversion of glucose to HMF. *Zhang* et al.[30] have tested different Brønsted acids and obtained 33% HMF yield using maleic acid and $AlCl_3$ catalyst in a single phase. *Wrigstedt* et al.[29] have investigated different salts and achieved 47% HMF yield using KBr and $CrCl_3$ catalyst in a biphasic system. *Swift* et al.[31] have obtained HMF yield over 50% using $CrCl_3$ and HCl catalyst in a biphasic system and developed a kinetic model. Moreover, the role of different metal salts, such as $CrCl_3$ and $AlCl_3$, in the production of HMF has also been investigated.[24, 35-39] *Norton* et al.[38] have investigated the speciation of Al(III) species and found that the soluble Al(III) ions form quickly, while the $Al(OH)_3$ solids form after extended heating, leading to a drop in catalytic activity due to the active species being removed from solution. *Choudhary* et al.[24] have investigated the speciation of Cr(III) ions and identified $[Cr(H_2O)_5(OH)]^{2+}$ as the catalytically active species for glucose isomerization. They also proposed that preheating of the catalyst is important to establish equilibration among species. However, little is known about the dynamic of Cr-related species forming under reaction conditions. Understanding the Cr(III) speciation and the impact on catalytic activity becomes even more important at short residence times where reaction and catalyst speciation time scales can be comparable. Moreover, these changes have not been taken into account in the previous kinetic models.[31]

In this work, we characterize the chromium species formed under reaction conditions using UV-Visible spectrophotometry (UV-Vis) and perform reactivity measurements in a flow microreactor at nearly isothermal conditions and short residence times. Then, we develop a kinetic model to describe the dynamics of Lewis and Brønsted acid catalyst speciation under reaction conditions and build a kinetic model that couples catalyst speciation with Lewis and Brønsted acid-catalyzed reactions using a hierarchical approach. Finally, we apply this model to maximize the yield of HMF.

Methods

Materials

Glucose (≥99% purity, Sigma Aldrich), fructose (≥99% purity, Sigma Aldrich), mannose (≥99% purity, Sigma Aldrich), chromium chloride hexahydrate (≥99% purity, Sigma Aldrich), hydrochloric acid (37 wt%, Fisher Scientific), and sulfuric acid (5M, Fluka), were used without further purification. All aqueous solutions were prepared using deionized (DI) water obtained using a Millipore water purification system (model: Direct-Q3 UV R).

Experimental setup

To carry out kinetic study of glucose conversion, reactions are conducted in a flow microreactor built in our laboratory as described by Desir et al.[17] The configuration of the reactor is provided in the Supporting Information (SI). Due to the much shorter heating time compared to the reaction time, no preheating of the catalyst was used for experiments with residence times longer than or equal to five min. On the other hand, the catalyst was preheated for the experiments with residence times less than five min.

In the former case, a mixture of sugars and catalyst was prepared in one feed reservoir. A Teledyne SSI MX reciprocating pump with Poly Ether Ether Ketone (PEEK) wetted internal parts was used to deliver the feed into a 1.5 m PEEK tube with 0.02 cm^2 cross-sectional area placed in an oven with temperature control (accuracy: ±1 °C). This PEEK tubing maximum working temperature of 250 °C and the pressure rating of 5,000 psi are sufficient for this work. In the latter case, two pumps were used. One pump (Teledyne SSI-MX) is connected to a reservoir containing a 2 wt% aqueous glucose feed. The other pump (Teledyne SSI-LS) is connected to the catalyst feed where the catalyst concentration is twice that used for the reaction. The catalyst feed enters a preheating coil of 1.5 m in length and a total volume of 3 mL. The sugars' feed is preheated for 30 seconds in a PEEK tube of 0.02 cm^2 cross-sectional area and variable-length to keep the preheating time constant. Control experiments showed that the conversion of 1 wt% glucose at 200 °C and 1 min of residence time without catalysts is minimal (less than 2%). Therefore, reactions of glucose in the preheating section can be neglected. This preheated glucose stream is mixed with the preheated catalyst feed at a T-junction. The flow rate ratio of the two streams is 1:1 so that the combined stream contains 1 wt% of glucose and the target catalyst concentration. The combined stream enters a coiled PEEK tube of 1 m length and 0.2 mL in total volume.

The reaction mixture exits the tube and immediately enters a coiled, thin PEEK tube with 0.002 cm^2 cross-sectional area placed in an ice-water bath to rapidly quench the chemistry. A stainless-steel 316 pressure gauge in the range of 0-1000 psi was installed after the quenching section to indicate the system pressure, and the product mixture was quenched to room temperature before entering the pressure gauge. The pressure gauge was the only stainless-steel part in the flow path,

and the internals were coated with molybdenum to prevent corrosion. A PEEK back-pressure regulator (BPR) was connected further downstream to pressurize the system and prevent vaporization. The back pressure used in the experiments was 250 psi, which is greater than the bubble point pressure of the water/HCl mixture at 200 °C and sufficient to maintain it in the subcooled phase. The eluents from the BPR were filtered and collected for High-Performance Liquid Chromatography (HPLC) analysis. The experimental conditions for kinetic study are listed in Table 1.

Aside from the experiments in Table 1 that are used for kinetics, experiments with varying catalyst heating times are also conducted. The catalyst heating experiments are first conducted in the absence of a substrate to investigate the effect of heating on catalyst speciation. Then, the glucose conversion experiments are conducted using catalyst with different heating times to investigate the effect of heating on catalyst reactivity. Experiments with heating time less than 1 hour were conducted in the continuous flow reactor as described previously, and those with heating time longer than 1 hour were done in thick-walled glass vial reactors (Sigma-Aldrich) 5 mL in volume. 2 mL of reacting mixture and a stir bar were placed in each vial. Then each vial was sealed with a crimp cap. To prevent water vapor leakage, a stainless-steel shim was inserted between each aluminum cap and the rubber septum. Then the vials were immersed in an aluminum heating block with individual vial slots filled with mineral oil pre-heated to the set point temperature. A thermocouple inserted into a vial filled with mineral oil sitting in the bath was used to monitor the actual temperature. The stirring rate was 500 rpm. Time zero was defined at the time when the vial was put into the oil bath. At each desired time point, a vial was taken out of the oil bath and immediately immersed in an ice-water bath to quench the reaction.

Product analysis

A Waters 2695 HPLC equipped with a RID and an Aminex Biorad 87C column heated at 75 °C was used for the determination of the glucose, mannose, and fructose concentrations. The mobile phase was deionized (DI) water at 0.5mL/min flow rate. The same samples were also run on a Waters 2695 HPLC equipped with a RID and an Aminex Biorad 87H column heated at 50 °C for determination of the acids and HMF concentration. The mobile phase was 0.005 mM of aqueous H_2SO_4 solution at 0.5 mL/min flow rate. External calibration standards were used in both cases. Reactant conversion and yields of identified products were calculated as follows:

$$Conversion\ [\%] = \frac{c_{reactant}^{t=0} - c_{reactant}}{c_{reactant}^{t=0}} \times 100\%$$

$$Yield_i\ [\%] = \frac{c_i}{c_{reactant}^{t=0}} \times 100\%$$

Characterization of Cr(III) species

UV-Vis analysis was conducted on a Cary 600 UV-Visible spectrophotometer. All scans were performed in the 200-800 nm range. DI water was used for 100% transmission baseline reference and zero absorbance calibrations. All samples were directly put into a 1 cm pathlength cuvette and inserted into the sample holder for analysis.

Kinetic models, experimental conditions, and parameter estimation

We use a hierarchical approach, proposed years ago,[40-42] to develop a complex kinetic model for glucose conversion over tandem Brønsted/Lewis-acid catalysts. In this method, we develop kinetic submodels, which usually consist of different building blocks, and integrate them together to build a full kinetic model. A building block typically describes the sub-network starting from a different substrate. Each building block is often described by a set of coupled ordinary differential equations (ODEs) describing the change of species involved in that building block with reaction time in a batch reactor or location in a plug flow reactor. Networks that involve a single substrate are modeled first, and their parameters are used as initial estimates (*priors*) for networks involving two or more substrates. Additional reactions are often needed to couple these building blocks. Rate constants are described via the Arrhenius equation to include temperature dependence. The temperature dependence of the equilibrium constant is described using the van't Hoff equation. All the reaction rates are first order on catalyst activity and substrate concentration.[31]

There are three main submodels in the reaction network: the Lewis acid-catalyzed reaction model, the Brønsted acid-catalyzed reaction model, and the catalyst speciation model, which affects the reaction kinetics. In the Lewis and Brønsted acid-catalyzed reaction model, there are multiple building blocks, namely the glucose, fructose, mannose, and HMF conversion sub-networks. All of them are developed separately using different datasets, as shown in Table 1. The catalyst speciation model describes the real-time Brønsted and Lewis acid species concentration vs. time and temperature, and the species considered in this model are discussed in detail in the *Results and Discussion*. The catalytically active Lewis species ($[Cr(H_2O)_5(OH)]^{2+}$) activity is determined from the $[Cr(H_2O)_5(OH)]^{2+}$ concentration obtained from the catalyst speciation model with an empirical representation developed by *Swift* et al.[31] The Brønsted acid catalyst activity is determined from the pH. Then, the catalyst speciation model is integrated with each reaction building block, as shown in Scheme 1, to calculate the concentrations of catalysts, reactants and products.

Experimental data is used to estimate kinetic parameters. There are two kinetic parameters for each reaction, namely the pre-exponential factor and the activation energy. To determine the parameters for each model, the normalized sum of the squared error between the estimated and the observed outlet concentration for different conditions in the training dataset is minimized. The open-source package, SciPy,[43] in Python is used to estimate the kinetic parameters. In Table 1, experiments 1–16 are used for parameter estimation (training set), and experiments 17–26 are reserved for model assessment (testing set). Specifically, the parameters of Brønsted acid-catalyzed mannose conversion and fructose dehydration are obtained from previous literature,[31, 44] and that of direct glucose conversion are estimated using experiments 10–16 (Table 1). The parameters of the catalyst speciation and Lewis acid-catalyzed reactions are estimated simultaneously using experiments 1–9 (Table 1).

Table 1. Experimental conditions employed for kinetic studies of glucose conversion. Experiments 1–16 are used for training and the rest for validation. All of the experiments are conducted in the continuous flow reactor with respect to different residence times between 0 to 60 min.

Experiment	Temperature [°C]	Substrate	Catalyst
1	140	Glucose (1 wt%)	1.7 mM $CrCl_3$

2	160	Glucose (1 wt%)	1.7 mM $CrCl_3$
3	180	Glucose (1 wt%)	1.7 mM $CrCl_3$
4	180	Mannose (1 wt%)	1.7 mM $CrCl_3$
5	200	Mannose (1 wt%)	1.7 mM $CrCl_3$
6	180	Fructose (1 wt%)	1.7 mM $CrCl_3$
7	200	Fructose (1 wt%)	1.7 mM $CrCl_3$
8	160	HMF (1 wt%)	1.7 mM $CrCl_3$
9	180	HMF (1 wt%)	1.7 mM $CrCl_3$
10	140	Glucose (1 wt%)	0.02 M HCl
11	160	Glucose (1 wt%)	0.02 M HCl
12	140	Glucose (1 wt%)	0.1 M HCl
13	160	Glucose (1 wt%)	0.1 M HCl
14	180	Glucose (1 wt%)	0.1 M HCl
15	160	Glucose (1 wt%)	0.056 M HCl
16	180	Glucose (1 wt%)	0.056 M HCl
17	160	Glucose (1 wt%)	0.03 M HCl
18	180	Glucose (1 wt%)	0.03 M HCl
19	180	Glucose (1 wt%)	0.01 M HCl
20	200	Glucose (1 wt%)	0.01 M HCl
21	180	Glucose (1 wt%)	1.7 mM $CrCl_3$ + 0.01 M HCl
22	200	Glucose (1 wt%)	1.7 mM $CrCl_3$ + 0.01 M HCl
23	180	Glucose (1 wt%)	1.7 mM $CrCl_3$ + 0.1 M HCl
24	200	Glucose (1 wt%)	1.7 mM $CrCl_3$ + 0.1 M HCl
25	200	Glucose (1 wt%)	1.7 mM $CrCl_3$ + 0.056 M HCl
26	200	Glucose (1 wt%)	1.7 mM $CrCl_3$ + 0.071 M HCl

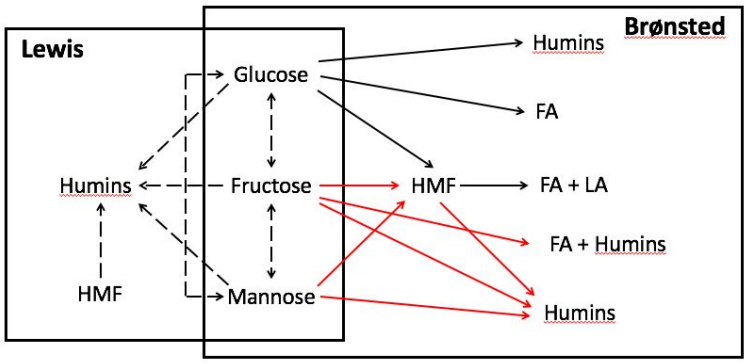

Scheme 1. Reaction network for glucose conversion including the Brønsted acid-catalyzed (solid lines) and the Lewis acid-catalyzed (dashed lines) pathways. The reaction network consists of four substrates, glucose, fructose, mannose, and HMF. Byproducts include formic acid (FA), levulinic acid (LA), and humins. The kinetic parameters of reactions with red lines are obtained from the literature, and those with black lines are estimated in this work.

Results and Discussion

Catalyst speciation and dynamics

It is important to understand the change of Cr(III) speciation and catalyst reactivity under different conditions, especially at short residence times and high temperatures, which are needed for process intensification. It is known that the chromium (III) hexaaquo complex $[Cr(H_2O)_6]^{3+}$ (referred to hereafter as Cr^{3+}) forms after $CrCl_3$ is dissolved in water (R_1).[45-47] Hydrolysis of Cr^{3+} forms $[Cr(H_2O)_5(OH)]^{2+}$ (referred to hereafter as $Cr(OH)^{2+}$), which is believed to be the catalytically active species for glucose isomerization[24] (R_2). Then, the $Cr(OH)^{2+}$ is further hydrolyzed and forms $Cr(OH)_3$ solids (R_3). During hydrolysis, protons that catalyze the dehydration reaction are also released. These reactions control the Lewis and Brønsted acid catalyst concentrations. In Figure 1, the key Cr(III)-related species equilibrium distribution at different temperatures in aqueous media is obtained from the OLI software, which is a commercial software based on an aqueous electrolyte model (OLI, 2018).[48] The Cr^{3+}, $Cr(OH)^{2+}$, and $Cr(OH)_3$ species account for most of the Cr (>98%). The species distribution greatly depends on the temperature. As the temperature increases, formation of the solids becomes more pronounce, at the expense of $Cr(OH)^{2+}$ leading to catalyst deactivation. Therefore, it's important to understand the Cr(III) speciation under different heating times.

$$CrCl_3 + 6H_2O \leftrightarrow [Cr(H_2O)_6]^{3+} + 3Cl^- \quad (R_1)$$

$$[Cr(H_2O)_6]^{3+} + H_2O \overset{k_2}{\leftrightarrow} [Cr(H_2O)_5(OH)]^{2+} + H_3O^+ \quad (R_2)$$

$$[Cr(H_2O)_5(OH)]^{2+} + 2H_2O \overset{k_3}{\leftrightarrow} Cr(OH)_{3(s)} \cdot 3H_2O_{(s)} + 2H_3O^+ \quad (R_3)$$

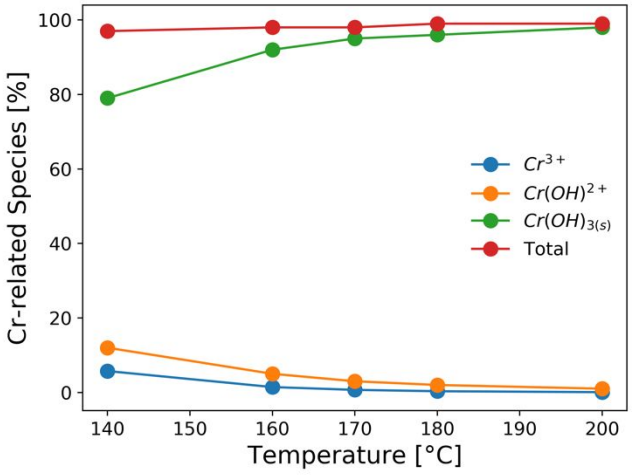

Figure 1. Effect of temperature on the species distribution at equilibrium of 1.7 mM $CrCl_3$ solution (calculated using the OLI software) in aqueous media.

The catalyst is heated for various times in the absence of a substrate to understand the Cr(III) speciation. To qualitatively follow the progress of Cr(III) speciation in water, we employ UV-Vis.

A 3.4 mM $CrCl_3$ solution, which is chosen to increase the sample absorption for detection by UV-Vis, is heated for different times. The UV-Vis spectra of the freshly prepared $CrCl_3$ solution shown in Figure 2 agree well with those by *Onjia* et al.[46] The spectra exhibit three peaks: a broad and intense peak between 200 and 300 nm (Peak 1), which corresponds to at least one pair of negative ligands coordinated in trans-positions,[49] and two much less intense peaks centers at 443 (Peak 2) and 633 nm (Peak 3), which correspond to the d−d transitions between different levels split from the d-orbital set of Cr^{3+}.[50, 51] Additionally, the shoulder at 692 nm is assigned to $[Cr(H_2O)_2Cl_4]^-$ by *Elving* et al.[50] After just 0.6 min of heating at 140 °C, a blue shift (i.e., a shift of peak positions to lower wavelengths) is observed for peaks 2 and 3. This is consistent with the color of the solution turning from bright green due to $[CrCl_4]^{2-}$ to a more bluish color associated with $[Cr(H_2O)_6]^{3+}$.[52] At the same time, the intensity of peak 1 reduces significantly. According to *Tsuchida* et al.[49], the $[Cr(H_2O)_6]^{3+}$ does not have any pairs of negatively charged coordinated ligands and therefore should not show an absorption peak in the ultraviolet region. The disappearance of peak 1 and of the shoulder at 692 nm after 0.6 min of heating is consistent with the complete replacement of coordinated Cl^- ions by water molecules (R_1). As the heating time becomes longer, peak 1 regrows in intensity with a different shape than that of the freshly prepared solution. This points to the formation of new electronic transitions arising from most likely an $[Cr(H_2O)_4(OH)_2]^+$ ion. We are not able to predict changes in the concentration of the catalytically active $[Cr(H_2O)_5(OH)]^{2+}$ species (R_2) using the UV-Vis technique since this ion does not have any pairs of coordinated negative ions associated with peak 1. However, we postulate that $[Cr(H_2O)_5(OH)]^{2+}$ ions form earlier and are transformed into $[Cr(H_2O)_4(OH)_2]^+$ ions, as the amount of $[Cr(H_2O)_4(OH)_2]^+$ ions increases, and are finally transformed into solids (R_3). On the other hand, the positions of peaks 2 and 3 are overall very similar for heating times longer than 0.6 min. Peaks 2 and 3 red-shift by 11 nm and 16 nm upon heating for 0.6 min and 24 hours, respectively, pointing to the formation of Cr species coordinated with more OH^- ions. According to studies on the effect of anion coordination in the UV-Vis spectra of transition metal complexes,[49] replacing a H_2O ligand with an OH^- could cause a slight red shift of the UV-Vis peak in the 350-800 nm region. This again indicates that the hydrolysis of $[Cr(H_2O)_6]^{3+}$ is happening. Apart from peak-position changes, the intensity of peaks 2 and 3 decreases from 0 to 0.6 min of preheating and increases at longer heating times. The change in absorbance also implies a change in Cr speciation, which needs to be considered while developing the kinetic model. Overall, the qualitative analysis of UV-Vis data supports the dynamic nature of the catalyst speciation, consistent with the mechanism (R_1–R_3) described above.

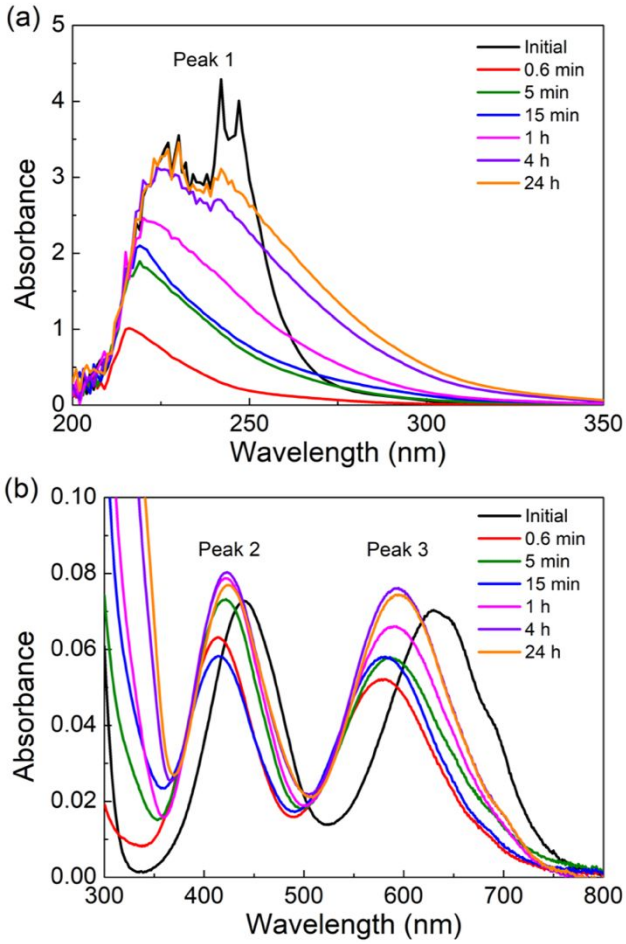

Figure 2. UV-Vis spectra of a freshly prepared 3.4 mM $CrCl_3$ solution and of the same solution heated at 140 °C at different times. (a) Low wavelengths (200-350 nm) and (b) high wavelengths (300-800 nm).

The catalyst solution in the absence of a substrate is also heated for various times, and the pH under different conditions is measured, as shown in Figure 3. This data is used to assess the catalyst speciation model in a later section. At all temperatures, the pH drops rapidly within the first 10 min and decreases gradually at longer residence times, indicating that there are two time scales. A shorter one, which controls speciation of small ions and the pH, pointing to the hydrolysis of Cr^{3+} ions following R_2, and consistent with the UV-Vis data (Figure 2), and a longer one that is controlled by the growth of solid particles accordingly to R_3. The two time scales for $CrCl_3$ are reminiscent of the $AlCl_3$ findings.[38] The color of the solution is light green at the beginning but becomes slightly bluish after an hour of preheating (Figure 3). After ultracentrifugation at 10,000 rpm for 10 min, the permeate became almost colorless but the retentate kept the green-bluish color. It can be concluded that green colloidal particles form upon heating the $CrCl_3$ solution, consistent with prior literature findings.[24, 46] Dynamic light scattering (DLS) experiments were attempted aiming at measuring the size of these particles, but due to the sample absorbing visible light at 532

nm, which is the wavelength of the laser of the DLS instrument, the Cr ions gave artifact background signals and unreliable autocorrelation functions.

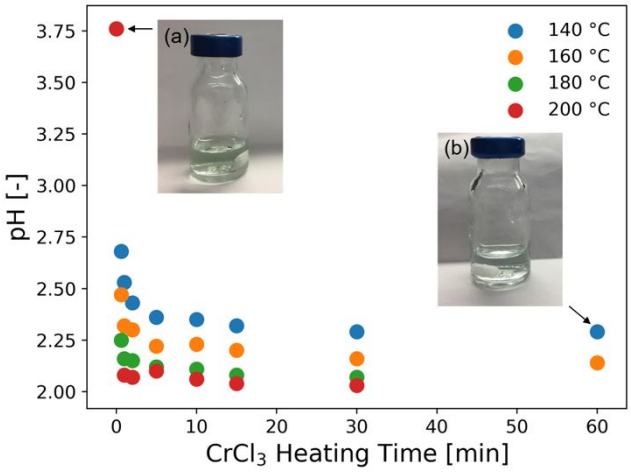

Figure 3. Catalyst heating experiments without substrates. Measured pH of a 3.4 mM $CrCl_3$ solution as a function of heating (residence) time at temperatures indicated. The pictures are of (a) freshly prepared $CrCl_3$ solution and (b) a $CrCl_3$ solution after preheating at 140 °C for an hour. Experiments were conducted in a flow microreactor.

Effect of heating on catalyst deactivation and reactivity

$CrCl_3$ solutions preheated from 0 to 24 hours are used for glucose conversion to probe the effect of speciation on reactivity. In Figure 4a, the glucose conversion decreases when increasing catalyst preheating time, up to 3 times upon 24 h catalyst preheating, indicating that the catalyst reactivity continues dropping despite the change in pH being slight. The HMF yield slightly decreases as well. These findings indicate gradual removal of the catalytically active species from solution due to formation of solids. When the reaction time (45 min in these experiments) is around the same or longer than the catalyst preheating time, the catalytically active species change noticeably during reaction.

To further investigate the effect of externally added Brønsted acidity, the HCl is added into the $CrCl_3$ solutions and preheated together. In Figure 4b, preheating a mixture of HCl and $CrCl_3$ with a pH = 1 for various times does not appreciably affect either the glucose conversion or the HMF yield, indicating that there is no significant change in reactivity. This is attributed to the Brønsted acid reducing the $CrOH^{2+}$ concentration via R_2 and suppressing the formation of solids, i.e., by eliminating R_3. Consequently, the reactivity of glucose in the presence of HCl is reduced to about half of that of the fresh $CrCl_3$ catalyst without added HCl and is double of the one when the $CrCl_3$ catalyst alone is heated for 24 hours (Figure 4a), i.e., the effect of HCl on glucose conversion can be detrimental, compared to using Lewis acid catalyst alone, or beneficial, due to avoiding catalyst solid formation. Further, the amount of HCl would play a role due to modifying the extent of reactions R_2 and R_3. We return to this point by optimizing the ratio of Lewis and Bronsted acids below.

To understand the reversibility of forming solids according to the reverse reaction of R_3, we preheated a 3.4 mM $CrCl_3$ solution for 24 hours at 140 °C. After cooling down this solution to room temperature, HCl was added to bring the solution pH to 1. Then, glucose was added in a 1:100 mass ratio (glucose : catalyst solution) and transferred to a temperature-controlled oil bath kept at 140 °C for 45 min. Compared to using a freshly prepared/non-preheated $CrCl_3$/HCl catalyst mixture, this $CrCl_3$/HCl catalyst gives significantly lower glucose conversion and HMF yield (Figure 4c). When HCl is added prior to catalyst heating (Figure 4b), the reactivity is higher as HCl prevents the formation of solids according to R_3. This suggests that upon $CrCl_3$ preheating, solids likely form by condensation of the $[Cr(H_2O)_x(OH)_y]^{3-y}$ species.[45, 53, 54] Once formed, the dissolution of the solids is slow, i.e., the process appears to be irreversible under typical reaction conditions and laboratory operation times.

Our results indicate that the catalyst treatment plays a vital role in getting optimal reactivity. While typical batch experiments are conducted over long reaction times, the residence time of continuous processes operating at high temperature can be orders of magnitude shorter, necessitating understanding of catalyst treatment or more commonly time in use because the catalyst changes rapidly. Moreover, since a catalyst in a continuous process is used for long times, catalyst deactivation, analogous to sintering of heterogeneous catalysts, is unavoidable and requires recording of the catalyst history.

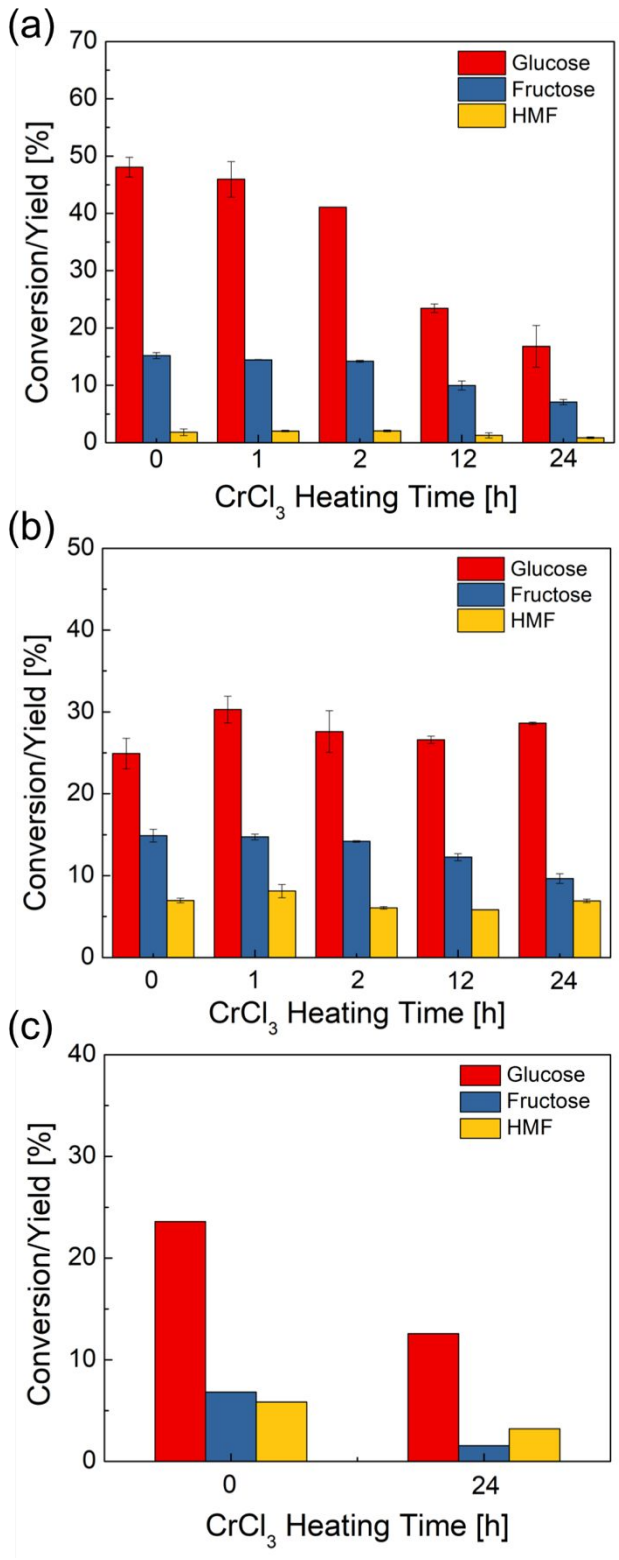

Figure 4. Glucose conversion and fructose and HMF yields as a function of $CrCl_3$/HCl catalyst preheating time. Reaction conditions: 1 wt% glucose at 140 °C for 45 min using 3.4 mM $CrCl_3$ catalyst with (a) no HCl (starting pH=3.76), (b) 0.1 M HCl (pH=1), and (c) $CrCl_3$ preheated for 0

or 24 h before adding HCl to a solution to bring pH to 1. Error bars were obtained from two repeat experiments for each set of conditions. The preheating and the reactions are performed in a batch reactor due to the need to preheat $CrCl_3$ catalyst for long time.

Kinetic studies on catalyst speciation and glucose conversion

Even though it is difficult to directly measure the active species concentration, it is important to model how they change during pretreatment and reaction of glucose to HMF. Therefore, we develop a simple kinetic model to account for the observed effect of heating on catalyst speciation. The catalyst speciation model is composed of two key reactions: the hydrolysis reaction (R_2) of Cr^{3+} to form the main catalytic active species $Cr(OH)^{2+}$, and the formation of solids $Cr(OH)_3$ (R_3), where formation of solids mostly happens at low H^+ concentration[55] and is greatly suppressed at high H^+ concentration. For simplicity, we assume that HCl fully dissociates in solution and Cr^{3+} ions form immediately upon dissolving $CrCl_3$ in water, with complete replacement of coordinated Cl^- ions by water molecules happening shortly, as observed in the UV-Vis spectra. The equations of the model are provided in the SI.

The catalyst speciation kinetic model is integrated with Lewis and Brønsted acid-catalyzed reactions to establish the full reaction network. The tandem kinetic model is developed based on the network proposed by *Swift* et al.[31], as shown in Scheme 1. The direct Brønsted acid-catalyzed pathway conversion of glucose to HMF has recently been studied[56-58] and is responsible for the ratio of formic acid (FA) to levulinic acid (LA) being greater than unity, compared to 1 when HMF rehydration occurs alone. *Yang* et al.[23] proposed that the additional FA stems from glucose retro-aldol reaction at high temperatures. This direct pathway along with the catalyst speciation are included in a new kinetic model herein for the first time.

The full reaction network is developed hierarchically. When only Brønsted acid catalyst (HCl) is present, the H^+ concentration is determined from the concentration of the acid (unaffected by Cr speciation). Therefore, first the unknown kinetic parameters of the Brønsted acid-catalyzed reaction model (black solid lines in Scheme 1) are estimated using experiments 10–16 in Table 1. On the other hand, since direct measurement of catalytically active Lewis species and solids is infeasible, we use glucose kinetics data to model both the sugar chemistry and the catalyst Cr speciation at once, i.e., the kinetic parameters of both models are estimated simultaneously. The procedure is iterative: the ODEs of four key species concentrations based on R_2 and R_3, namely Cr^{3+}, $Cr(OH)^{2+}$, $Cr(OH)_3$, and H^+, are first formulated and solved in a plug flow reactor with respect to residence time. Then, the concentrations of catalytically active species, $Cr(OH)^{2+}$ and H^+, are passed into the glucose kinetics model as Lewis and Brønsted acid catalyst concentrations, respectively, and used to solve the concentration profiles for glucose, fructose, mannose, HMF, FA, and LA. The calculated concentration profiles of aforementioned species are compared with experiments 1–9 (Table 1) to estimate the kinetic parameters of both catalyst speciation model (R_2 and R_3) and Lewis-acid catalyzed reaction model (dashed solid lines in Scheme 1) and the approach is iterated until numerical convergence in kinetic parameters is achieved. The method of estimating the kinetic parameters is mentioned in the *Methods* section. The model can account for preheating by simulating the catalyst speciation without a substrate and also for the coupled catalyst and reaction dynamics. The estimated parameters of the catalyst speciation model are shown in Table 2, and that of Brønsted- and Lewis-acid catalyzed reaction model are shown in

Table 3. Figure 5 shows a parity plot using the data reserved for model assessment (experiments 17–26 in Table 1). The model predictions are in good agreement with experiments for most cases, and the relative error is at most 30%, indicating the catalyst speciation model is adequate.

Table 2. Estimated kinetic parameters of the catalyst speciation model.

	Activation energy E_a [kJ/mol]	Pre-exponential factor $\log_{10}$ [A_0, 1/min]
k_2	96 ± 4	12.2
k_3	85 ± 6	8.9

[a]Reverse reactions are modeled using the equilibrium constants obtained from the OLI software. The equilibrium constants are provided in the SI.

Table 3. Estimated or literature kinetic parameters for reactions shown in Scheme 1.

Reaction	Catalyst	Activation energy E_a [kJ/mol]	Pre-exponential factor $\log_{10}$ [A_0, 1/min]
Glucose → fructose[a]	$CrCl_3$	73 ± 6	8.1
Fructose → mannose[a]	$CrCl_3$	75 ± 3	7.8
Mannose → glucose[a]	$CrCl_3$	80 ± 9	8.1
Fructose → humins	$CrCl_3$	71 ± 8	8.1
Mannose → humins	$CrCl_3$	110 ± 8	11.1
Glucose → humins	$CrCl_3$	73 ± 10	6.8
HMF → humins	$CrCl_3$	55 ± 8	4.2
Mannose → HMF[b,31]	HCl	17 ± 3	20.5
Mannose → humins[b,31]	HCl	58 ± 12	5.6
Fructose → HMF[b,44]	HCl	127 ± 2	18.1
Fructose → humins[b,44]	HCl	133 ± 7	16.4
HMF → humins[b,44]	HCl	64 ± 8	6.6
Fructose → FA/humins[b,44]	HCl	129 ± 10	15.5
HMF → LA/FA	HCl	92 ± 5	11.0
Glucose → HMF	HCl	139 ± 4	15.6
Glucose → FA	HCl	180 ± 10	17.7
Glucose → humins	HCl	183 ± 3	20.3

[a]Parameters of reverse reactions are calculated using literature equilibrium constants.[59]
[b]Parameters are obtained from literature as cited.

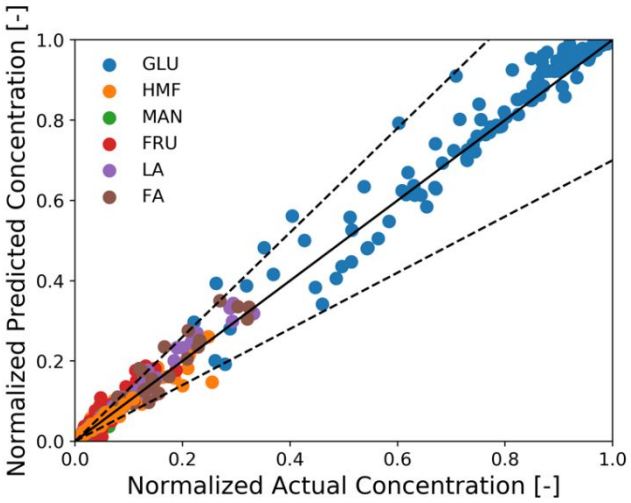

Figure 5. Parity plot of normalized concentration predicted by the model and obtained from experiments. Solid line is the parity line; points are data reserved for model assessment; and dashed lines are 30% error lines.

The predicted catalyst speciation is shown in Figure 6. The model-predicted proton concentration is compared with the measured pH, previously shown in Figure 3. The rapid increase in the H^+ concentration (or drop in pH) is correctly captured by the model. A sharp peak in the $Cr(OH)^{2+}$ concentration is observed at very short times. An additional set of experiments (not listed in Table 1) is conducted at short residence times (3–20 s) so that the catalyst changes and the glucose conversion are low. In Figure 7, the resulting simulations agree well with experiments, indicating that the catalyst speciation model can adequately describe the dynamics of Lewis and Brønsted acid active species at short reaction times. A non-monotonic variation of initial glucose reaction rate vs. the $CrCl_3$ preheating time is observed in both simulations and experiments with an overall variation in reaction rate up to 3-4 times at these conditions. The initial glucose reaction rate reaches a maximum at ~1 min and then decreases. This behavior can be explained by the interplay between the hydrolysis of Cr^{3+} (R_2) and the formation of the $Cr(OH)_3$ solids (R_3). At short heating times (~3 min), Cr^{3+} is rapidly hydrolyzed to form $Cr(OH)^{2+}$ releasing protons, which is consistent with the pH rapidly dropping (Figure 3). At longer preheating times, the Cr^{3+} hydrolysis is either complete and/or the $Cr(OH)^{2+}$ starts forming solids, which lower the concentration of the active species and consequently the glucose reaction rate.

This indicates that one should carefully consider catalyst pretreatment compared to the operating time since the catalyst speciation happens rapidly in the first ~10 min of heating at 180 °C (Figure 6 and Figure 7). Specifically, if one performs the reaction at very short residence times (<< 10 min), preheating the catalyst for ~1 min can provide higher reaction rate. On the other hand, if the reaction is carried out at much longer residence times (>> 10 min), the effect of preheating catalyst is less significant since catalyst deactivation happens already during reaction. The catalyst dynamics can also affect reproducibility among different reports.

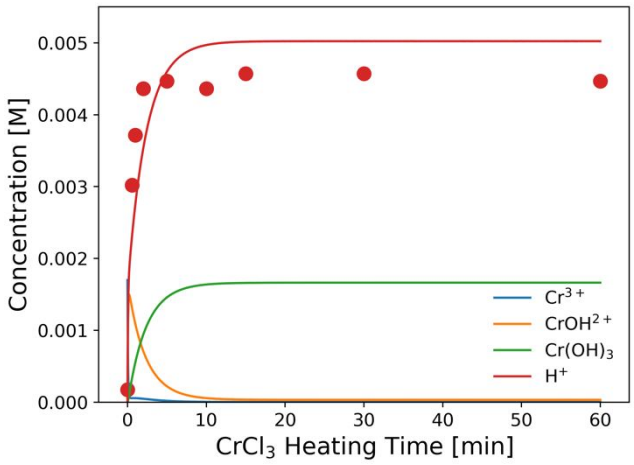

Figure 6. Concentrations of key catalyst species vs. preheating time at 180 °C. Circles are experimental data; lines represent model predictions. Conditions are those of Figure 3.

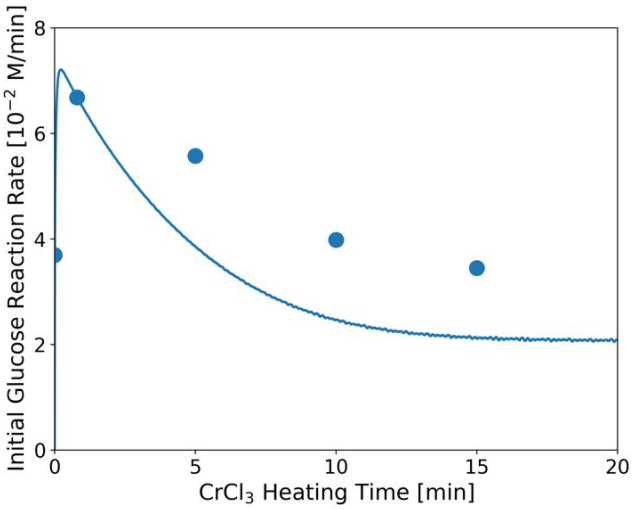

Figure 7. Glucose initial reaction rate over catalysts heated for different preheating times. Reaction conditions: 1 wt% glucose with 1.7 mM $CrCl_3$ at 180 °C. The catalyst was preheated in the flow reactor at the same temperature as that used for the glucose reaction. Circles are experimental data; line represents model prediction. The method for calculating the initial experimental glucose reaction rate at short times is provided in the SI.

Figure 8a shows the experimental conversion/yields (circles) and model predictions (lines) of the direct Brønsted acid-catalyzed reaction. The excess of FA becomes more pronounced as the glucose conversion increases but under these conditions the ratio of FA to LA is close to 1. While no literature is available for direct comparison, the estimated activation energy (180 kJ/mol) is high as expected for the retro-aldol reaction.[23] The other estimated activation energies are comparable to literature reported values.[56-58] Figure 8b shows conversion and yields of typical

Lewis-acid catalyzed reactions. The activation energies of glucose–fructose and fructose–mannose isomerization are similar, which may be attributed to that both reactions proceed via 1,2 intramolecular hydride transfer.[33, 60] Besides, the mannose-glucose isomerization activation energy is similar to the literature reported value,[31] while the activation energies of glucose–fructose and fructose–mannose are slightly lower, possibly due to the catalyst speciation.

The model is also assessed using the tandem Lewis/Brønsted-acid catalyst. Figure 9 shows the experimental conversion/yields (circles) and model predictions (lines). The conversion of glucose and the HMF yield increase much faster using the tandem Lewis/Brønsted-acid catalyst compared to using only the Lewis-acid catalyst. This is attributed to that the additional Brønsted-acidity, provided by HCl, promotes the fructose dehydration reaction and drives the equilibrium-limited glucose–fructose isomerization to high conversions by converting fructose. Besides, the formation of solids is suppressed by the addition of HCl. However, the additional HCl also shifts the hydrolysis reaction backward reducing the amount of catalytically active species $Cr(OH)^{2+}$[31] and thus decreasing the Lewis-acid catalyst activity. Given these tradeoffs, tuning the ratio of the two catalysts is important to determine the optimal reaction conditions.

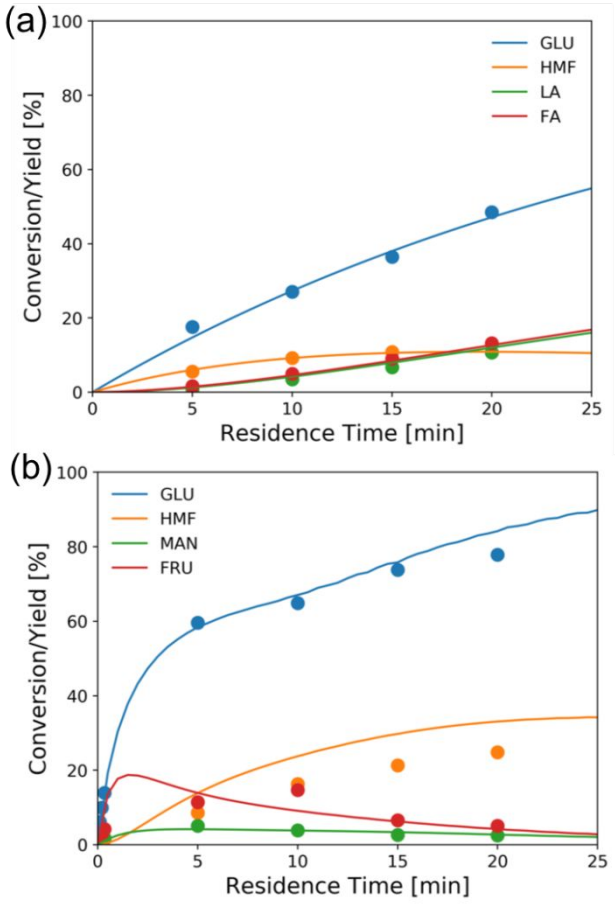

Figure 8. Conversion and yield of 1 wt% glucose vs residence time in (a) aqueous HCl (pH=2) at 200 °C and (b) 1.7 mM $CrCl_3$ at 180 °C from experiments (circles) and model predictions (lines).

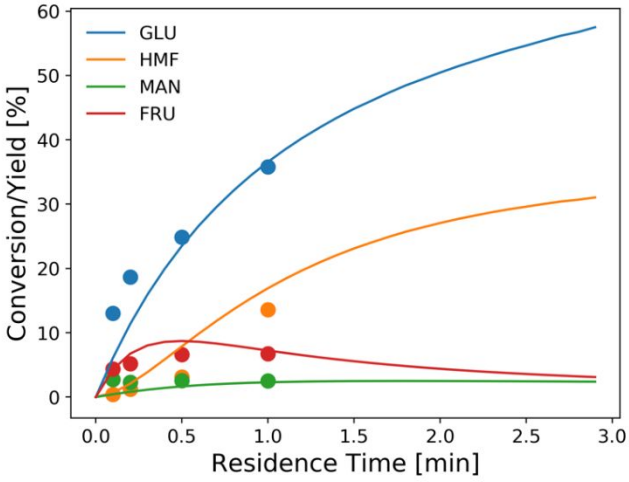

Figure 9. Conversion and yield of 1 wt% glucose vs residence time using 1.7 mM $CrCl_3$ in aqueous HCl (pH=2) at 200 °C from experiments (circles) and model predictions (lines).

Optimal HMF yield at short contact time using tandem $CrCl_3$/HCl catalyst

To find out the optimal reaction conditions for HMF production, first, parametric studies are carried out to investigate the effect of $CrCl_3$ concentration on HMF yield at 160 and 180 °C (Figure 10). The maximum HMF yield depends mainly on temperature and does not change with $CrCl_3$ concentration. It first increases and then decreases with increasing HCl concentration. This is attributed to the rate-limiting step changing from dehydration at low HCl concentrations to isomerization at high HCl concentrations,[31] indicating that the optimum happens by balancing the dehydration and isomerization rates. The optimal HCl concentration increases when the $CrCl_3$ concentration increases. Then, the model is applied to find out the operating window under various conditions. Figure 11 shows the heatmap of predicted HMF yield vs the residence time and HCl concentration with 1.7 mM $CrCl_3$ at different temperatures. The maximum HMF yield is ~36% at 200 °C in ~7 min and ~33% at 180 °C in ~15 min. These stand among the highest yields in single aqueous phase starting from glucose over $CrCl_3$ catalyst. There are very few literature works that use flow reactors at high temperature, and only *Muranaka* et al.[21] obtained ~40% HMF yield in 22 min at 180 °C using a PBS buffer (pH = 2) in a flow reactor (buffers often have catalytic activity themselves). Other relatively high yields have been obtained in a batch reactor by *Siqueira* et al.[61] (47% yield in 100 min at 200 °C using TiO_2-P) and *Watanabe* et al.[62] (20% HMF yield in 5 min using anatase TiO_2 at 200 °C), but batch systems suffer from long preheating times. More detailed comparison is not possible as catalysts have been different.

In comparison to literature, this study shows that moderately high HMF yields can be reached using a microreactor operating at short residence times and high temperatures. While a moderate HCl concentration gives a higher yield and a larger operating window, which is desirable from a control viewpoint, the optimal residence time greatly decreases when the HCl concentration increases with only a slight decrease in the optimal HMF yield. This results in more compact reactors with less capital cost for small scale operation. When considering both product yield and

operation time, the productivity, defined as the HMF yield per time, increases using higher HCl concentrations. In this context, an additional experiment is carried out using 1.7 mM $CrCl_3$ and 0.056 M HCl as catalyst at 200 °C at 2 min. A HMF productivity of 15.2% yield/min is achieved, which is slightly higher than the model-predicted productivity, as shown in Figure 12. This is the highest productivity among all studies[21, 30, 61-63] using flow reactors with single aqueous phase and the same initial glucose concentration (1 wt%). This high productivity at short contact times is attributed to both fast heat transfer of the microreactor and the effectiveness of the tandem $CrCl_3$/HCl catalysts.

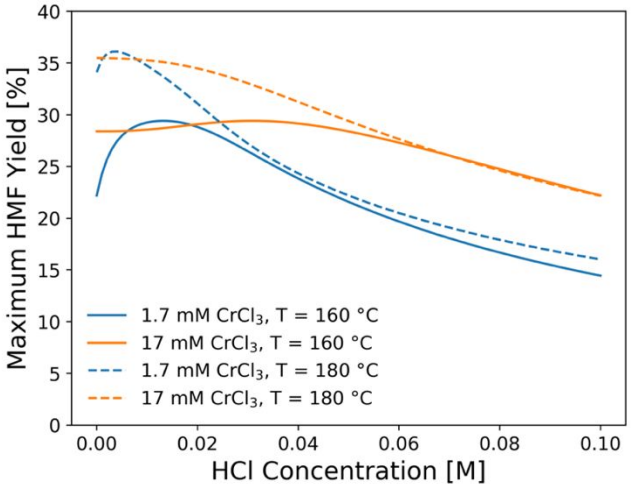

Figure 10. Maximum HMF yield obtained at optimal residence time as a function of HCl concentration at different $CrCl_3$ concentrations and temperatures.

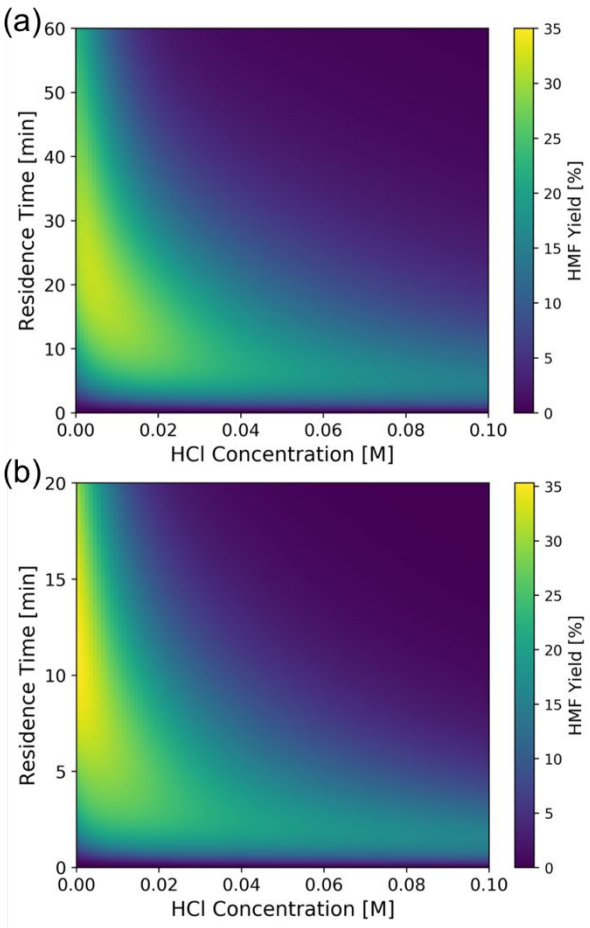

Figure 11. Model-predicted contour plot of HMF yield vs residence time and HCl concentration of 1 wt% glucose over 1.7 mM $CrCl_3$ at (a) 180 °C and (b) 200 °C.

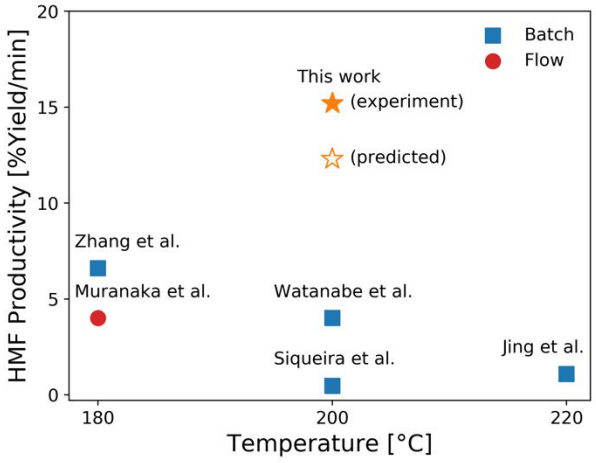

Figure 12. HMF productivity vs. temperature from this work and relevant literature[21, 30, 61-63]. All literature works used 1 wt% glucose solutions in single (aqueous) phase only.

Conclusions

HMF production from glucose via cascade reactions using Lewis acid ($CrCl_3$) and Brønsted acid (HCl) catalysts in aqueous media was investigated experimentally and computationally in a continuous flow microreactor at short residence times and high temperatures. We studied the chromium species formation at reaction-relevant conditions using UV-Visible spectrophotometry and elucidated the effect of Cr(III) speciation on glucose isomerization. A kinetic model for catalyst speciation was also developed via a hierarchical approach using experimental data and was coupled with a revised glucose isomerization and dehydration model that accounts for the varying catalyst speciation. The model is in good agreement with experiments at various reaction conditions.

It is found that there are two overall time-scales in Lewis acid catalyst speciation. At short heating times, Cr^{3+} is rapidly hydrolyzed to form $Cr(OH)^{2+}$ releasing protons, consistent with rapid drop of pH within minutes. At longer preheating times, the Cr^{3+} hydrolysis is either complete and/or the $Cr(OH)^{2+}$ starts forming solids and oligomers, which lower the concentration of the active species and consequently the glucose consumption rate. The catalyst reactivity changes sharply at short residence times; specifically, it goes through a maximum and eventually decreases at long heating or reaction times, fully rationalized by the varying catalyst speciation. The resulting catalyst activity changes with time by a factor of 3-4 (depending on conditions). Our results indicate that the Lewis acid catalyst treatment plays a vital role in getting optimal reactivity. Since a catalyst in a continuous process is used over long times, catalyst deactivation due to formation of particles is unavoidable. This behavior is analogous to sintering of heterogeneous catalysts. It appears that solid formation is irreversible by HCl treatment. Developing efficient catalyst regeneration methods should be pursued in future work. Adding Brønsted acids, e.g., HCl, reduces the Lewis acid active species at short times by reversing the hydrolysis reaction but prevents solids' formation at longer times and thus provides stable tandem catalyst speciation. It is clear that tandem catalysis has multiple benefits given that Brønsted acids shift the glucose-fructose equilibrium by accelerating fructose dehydration, reduce processing times, and increase HMF yield.

Finally, the model was applied to optimize the HMF yield and understand the interplay of processing conditions. The HMF yield is insensitive to the $CrCl_3$ concentration and depends primarily on temperature once residence time and HCl concentration are properly engineered. One of the highest yields (~36% at 200 °C in ~7 min) was predicted for a single-phase (aqueous) system, and the higher HMF productivity of 15.2% yield/min was experimentally demonstrated at short times (2 min). While the yield in a monophasic system is relatively low, the developed kinetics model can be applied directly to model and design a biphasic system for glucose conversion to HMF to further promote the product yield. The simplicity of the monophasic system studied herein enabled us to focus on catalyst speciation without complications arising from using an organic solvent. Moreover, the applied approach of modeling catalyst speciation and glucose conversion simultaneously can be extended to other homogeneous tandem catalyst systems. Changes in catalyst speciation may occur also in heterogeneous catalysts. The short contact times and good temperature control of the microfluidic enable studies of such changes. Continuous flow microreactors operating at short residence times and high temperatures can give high HMF productivity and contribute to process intensification of biorefineries. The combination of the developed kinetics model and computational fluid dynamics (CFD) simulation can further guide

the design of compact microreactor modules for HMF production and open up the possibility for small-scale and distributed biorefineries.

Conflicts of interest

There are no conflicts to declare.

Acknowledgments

Funding from the RAPID manufacturing institute, supported by the Department of Energy (DOE) Advanced Manufacturing Office (AMO), award numbers DE-EE0007888-7.6 is gratefully acknowledged. RAPID projects at the University of Delaware are also made possible in part by funding provided by the State of Delaware. The Delaware Energy Institute gratefully acknowledges the support and partnership of the State of Delaware in furthering the essential scientific research being conducted through the RAPID projects.

References

1. S. Caratzoulas, M. E. Davis, R. J. Gorte, R. Gounder, R. F. Lobo, V. Nikolakis, S. I. Sandler, M. A. Snyder, M. Tsapatsis and D. G. Vlachos, *The Journal of Physical Chemistry C*, 2014, **118**, 22815-22833.
2. B. J. Nikolau, M. A. D. N. Perera, L. Brachova and B. Shanks, *The Plant Journal*, 2008, **54**, 536-545.
3. R. J. van Putten, J. N. M. Soetedjo, E. A. Pidko, J. C. van der Waal, E. J. M. Hensen, E. de Jong and H. J. Heeres, *ChemSusChem*, 2013, **6**, 1681-1687.
4. J. Q. Bond, D. M. Alonso and J. A. Dumesic, *Aqueous Pretreatment of Plant Biomass for Biological and Chemical Conversion to Fuels and Chemicals*, 2013, 61-102.
5. O. A. Abdelrahman, H. Y. Luo, A. Heyden, Y. Román-Leshkov and J. Q. Bond, *Journal of Catalysis*, 2015, **329**, 10-21.
6. D. M. Alonso, J. Q. Bond and J. A. Dumesic, *Green Chemistry*, 2010, **12**, 1493-1513.
7. H. Xia, S. Xu, H. Hu, J. An and C. Li, *RSC Advances*, 2018, **8**, 30875-30886.
8. T. Ennaert, J. Van Aelst, J. Dijkmans, R. De Clercq, W. Schutyser, M. Dusselier, D. Verboekend and B. F. Sels, *Chemical Society Reviews*, 2016, **45**, 584-611.
9. E. Nikolla, Y. Román-Leshkov, M. Moliner and M. E. Davis, *Acs Catalysis*, 2011, **1**, 408-410.
10. R. Otomo, T. Yokoi, J. N. Kondo and T. Tatsumi, *Applied Catalysis A: General*, 2014, **470**, 318-326.
11. Y. J. Pagan-Torres, T. Wang, J. M. R. Gallo, B. H. Shanks and J. A. Dumesic, *Acs Catalysis*, 2012, **2**, 930-934.
12. Y. Román-Leshkov and J. A. Dumesic, *Topics in Catalysis*, 2009, **52**, 297-303.
13. H. Kimura, M. Nakahara and N. Matubayasi, *The Journal of Physical Chemistry A*, 2013, **117**, 2102-2113.
14. Y. Román-Leshkov, J. N. Chheda and J. A. Dumesic, *Science*, 2006, **312**, 1933-1937.
15. A. Hommes, H. J. Heeres and J. Yue, *ChemCatChem*, 2019, **11**, 4671-4708.
16. W. Guo, H. J. Heeres and J. Yue, *Chemical Engineering Journal*, 2020, **381**, 122754.

17. P. Desir, B. Saha and D. G. Vlachos, *Energy & Environmental Science*, 2019, **12**, 2463-2475.
18. P. Desir, T.-Y. Chen, M. Bracconi, B. Saha, M. Maestri and D. G. Vlachos, *Reaction Chemistry & Engineering*, 2020, **5**, 39-50.
19. T.-Y. Chen, M. Baker-Fales and D. G. Vlachos, *Industrial & Engineering Chemistry Research*, 2020.
20. T. Tuercke, S. Panic and S. Loebbecke, *Chemical Engineering & Technology: Industrial Chemistry-Plant Equipment-Process Engineering-Biotechnology*, 2009, **32**, 1815-1822.
21. Y. Muranaka, H. Nakagawa, R. Masaki, T. Maki and K. Mae, *Industrial & Engineering Chemistry Research*, 2017, **56**, 10998-11005.
22. F. Salak Asghari and H. Yoshida, *Industrial & Engineering Chemistry Research*, 2006, **45**, 2163-2173.
23. L. Yang, G. Tsilomelekis, S. Caratzoulas and D. G. Vlachos, *ChemSusChem*, 2015, **8**, 1334-1341.
24. V. Choudhary, S. H. Mushrif, C. Ho, A. Anderko, V. Nikolakis, N. S. Marinkovic, A. I. Frenkel, S. I. Sandler and D. G. Vlachos, *Journal of the American Chemical Society*, 2013, **135**, 3997-4006.
25. R. N. Goldberg and Y. B. Tewari, *Journal of Physical and Chemical Reference Data*, 1995, **24**, 1765-1801.
26. R. Bermejo-Deval, R. S. Assary, E. Nikolla, M. Moliner, Y. Román-Leshkov, S.-J. Hwang, A. Palsdottir, D. Silverman, R. F. Lobo and L. A. Curtiss, *Proceedings of the National Academy of Sciences*, 2012, **109**, 9727-9732.
27. H. Y. Luo, J. D. Lewis and Y. Román-Leshkov, *Annual Review of Chemical and Biomolecular Engineering*, 2016, **7**, 663-692.
28. C. Loerbroks, J. van Rijn, M. P. Ruby, Q. Tong, F. Schüth and W. Thiel, *Chemistry–A European Journal*, 2014, **20**, 12298-12309.
29. P. Wrigstedt, J. Keskiväli, M. Leskelä and T. Repo, *ChemCatChem*, 2015, **7**, 501-507.
30. X. Zhang, B. B. Hewetson and N. S. Mosier, *Energy & Fuels*, 2015, **29**, 2387-2393.
31. T. D. Swift, H. Nguyen, A. Anderko, V. Nikolakis and D. G. Vlachos, *Green Chemistry*, 2015, **17**, 4725-4735.
32. T. D. Swift, H. Nguyen, Z. Erdman, J. S. Kruger, V. Nikolakis and D. G. Vlachos, *Journal of catalysis*, 2016, **333**, 149-161.
33. Y. Román-Leshkov, M. Moliner, J. A. Labinger and M. E. Davis, *Angewandte Chemie International Edition*, 2010, **49**, 8954-8957.
34. S. Xu, D. Pan, F. Hu, Y. Wu, H. Wang, Y. Chen, H. Yuan, L. Gao and G. Xiao, *Fuel Processing Technology*, 2019, **190**, 38-46.
35. C. B. Rasrendra, I. Makertihartha, S. Adisasmito and H. J. Heeres, *Topics in Catalysis*, 2010, **53**, 1241-1247.
36. L. Peng, L. Lin, J. Zhang, J. Zhuang, B. Zhang and Y. Gong, *Molecules*, 2010, **15**, 5258-5272.
37. S. De, S. Dutta and B. Saha, *Green Chemistry*, 2011, **13**, 2859-2868.
38. A. M. Norton, H. Nguyen, N. L. Xiao and D. G. Vlachos, *RSC advances*, 2018, **8**, 17101-17109.
39. N. Rodriguez Quiroz, A. M. Norton, H. Nguyen, E. Vasileiadou and D. G. Vlachos, *ACS Catalysis*, 2019, **9**, 9923-9952.

40. A. B. Mhadeshwar and D. G. Vlachos, *The Journal of Physical Chemistry B*, 2005, **109**, 16819-16835.
41. A. B. Mhadeshwar and D. G. Vlachos, *Journal of Catalysis*, 2005, **234**, 48-63.
42. D. G. Vlachos, A. B. Mhadeshwar and N. S. Kaisare, *Computers & Chemical Engineering*, 2006, **30**, 1712-1724.
43. P. Virtanen, R. Gommers, T. E. Oliphant, M. Haberland, T. Reddy, D. Cournapeau, E. Burovski, P. Peterson, W. Weckesser, J. Bright, S. J. van der Walt, M. Brett, J. Wilson, K. J. Millman, N. Mayorov, A. R. J. Nelson, E. Jones, R. Kern, E. Larson, C. J. Carey, İ. Polat, Y. Feng, E. W. Moore, J. VanderPlas, D. Laxalde, J. Perktold, R. Cimrman, I. Henriksen, E. A. Quintero, C. R. Harris, A. M. Archibald, A. H. Ribeiro, F. Pedregosa, P. van Mulbregt, A. Vijaykumar, A. P. Bardelli, A. Rothberg, A. Hilboll, A. Kloeckner, A. Scopatz, A. Lee, A. Rokem, C. N. Woods, C. Fulton, C. Masson, C. Häggström, C. Fitzgerald, D. A. Nicholson, D. R. Hagen, D. V. Pasechnik, E. Olivetti, E. Martin, E. Wieser, F. Silva, F. Lenders, F. Wilhelm, G. Young, G. A. Price, G.-L. Ingold, G. E. Allen, G. R. Lee, H. Audren, I. Probst, J. P. Dietrich, J. Silterra, J. T. Webber, J. Slavič, J. Nothman, J. Buchner, J. Kulick, J. L. Schönberger, J. V. de Miranda Cardoso, J. Reimer, J. Harrington, J. L. C. Rodríguez, J. Nunez-Iglesias, J. Kuczynski, K. Tritz, M. Thoma, M. Newville, M. Kümmerer, M. Bolingbroke, M. Tartre, M. Pak, N. J. Smith, N. Nowaczyk, N. Shebanov, O. Pavlyk, P. A. Brodtkorb, P. Lee, R. T. McGibbon, R. Feldbauer, S. Lewis, S. Tygier, S. Sievert, S. Vigna, S. Peterson, S. More, T. Pudlik, T. Oshima, T. J. Pingel, T. P. Robitaille, T. Spura, T. R. Jones, T. Cera, T. Leslie, T. Zito, T. Krauss, U. Upadhyay, Y. O. Halchenko, Y. Vázquez-Baeza and C. SciPy, *Nature Methods*, 2020, **17**, 261-272.
44. T. D. Swift, C. Bagia, V. Choudhary, G. Peklaris, V. Nikolakis and D. G. Vlachos, *ACS Catalysis*, 2014, **4**, 259-267.
45. H. Stuenzi and W. Marty, *Inorganic Chemistry*, 1983, **22**, 2145-2150.
46. A. E. Onjia, S. K. Milonjić, D. Čokeša, M. Čomor and N. Miljević, *Materials research bulletin*, 2003, **38**, 1329-1339.
47. A. Bell and E. Matijević, *Journal of Inorganic and Nuclear Chemistry*, 1975, **37**, 907-912.
48. P. Wang, A. Anderko and R. D. Young, *Fluid Phase Equilibria*, 2002, **203**, 141-176.
49. R. Tsuchida, *Bulletin of the Chemical Society of Japan*, 1938, **13**, 388-400.
50. P. J. Elving and B. Zemel, *Journal of the American Chemical Society*, 1957, **79**, 1281-1285.
51. S. Jia, K. Liu, Z. Xu, P. Yan, W. Xu, X. Liu and Z. C. Zhang, *Catalysis Today*, 2014, **234**, 83-90.
52. A. Lennartson, *Nature chemistry*, 2014, **6**, 942-942.
53. F. P. Rotzinger, H. Stuenzi and W. Marty, *Inorganic Chemistry*, 1986, **25**, 489-495.
54. M. J. Avena, C. E. Giacomelli and C. P. De Pauli, *Journal of Colloid and interface science*, 1996, **180**, 428-435.
55. D. Rai, B. M. Sass and D. A. Moore, *Inorganic Chemistry*, 1987, **26**, 345-349.
56. R. Weingarten, J. Cho, R. Xing, W. C. Conner Jr and G. W. Huber, *ChemSusChem*, 2012, **5**, 1280-1290.
57. B. Girisuta, L. Janssen and H. J. Heeres, *Green Chemistry*, 2006, **8**, 701-709.
58. B. Girisuta, L. Janssen and H. J. Heeres, *Chemical Engineering Research and Design*, 2006, **84**, 339-349.
59. N. Rajabbeigi, A. I. Torres, C. M. Lew, B. Elyassi, L. Ren, Z. Wang, H. J. Cho, W. Fan, P. Daoutidis and M. Tsapatsis, *Chemical Engineering Science*, 2014, **116**, 235-242.

60. R. Bermejo-Deval, R. Gounder and M. E. Davis, *ACS Catalysis*, 2012, **2**, 2705-2713.
61. B. G. Siqueira, M. A. P. Silva and C. Moraes, *Brazilian Journal of Petroleum and Gas*, 2013, **7**, 71-82.
62. M. Watanabe, Y. Aizawa, T. Iida, T. M. Aida, C. Levy, K. Sue and H. Inomata, *Carbohydrate Research*, 2005, **340**, 1925-1930.
63. Q. Jing and X. LÜ, *Chinese Journal of Chemical Engineering*, 2008, **16**, 890-894.